

Behavior of a steel bridge with large caisson foundations under earthquake and tsunami actions

Lan Kang¹, Hanbin Ge^{*2}, Kazuya Magoshi³ and Tetsuya Nonaka⁴

¹ School of Civil Engineering and Transportation, South China University of Technology, Guangzhou, 510640, China

² Department of Civil Engineering, Meijo University, Nagoya, 468-8502, Japan

³ Seismic Analysis Research Inc. 3-21-19 Harunonisi Bld., Haruyoshi, Chuo-Ku, Fukuoka City, 810-0003, Japan

⁴ Nagoya Institute of Technology, Department of Civil Engineering, Nagoya, Aichi 466-8555, Japan

(Received July 26, 2018, Revised April 29, 2019, Accepted May 12, 2019)

Abstract. The main focus of this study is to numerically investigate the influence of strong earthquake and tsunami-induced wave impact on the response and behavior of a cable-stayed steel bridge with large caisson foundations, by assuming that the earthquake and the tsunami come from the same fault motion. For this purpose, a series of numerical simulations were carried out. First of all, the tsunami-induced flow speed, direction and tsunami height were determined by conducting a two-dimensional (2D) tsunami propagation analysis in a large area, and then these parameters obtained from tsunami propagation analysis were employed in a detailed three-dimensional (3D) fluid analysis to obtain tsunami-induced wave impact force. Furthermore, a fiber model, which is commonly used in the seismic analysis of steel bridge structures, was adopted considering material and geometric nonlinearity. The residual stresses induced by the earthquake were applied into the numerical model during the following finite element analysis as the initial stress state, in which the acquired tsunami forces were input to a whole bridge system. Based on the analytical results, it can be seen that the foundation sliding was not observed although the caisson foundation came floating slightly, and the damage arising during the earthquake did not expand when the tsunami-induced wave impact is applied to the steel bridge. It is concluded that the influence of tsunami-induced wave force is relatively small for such steel bridge with large caisson foundations. Besides, a numerical procedure is proposed for quantitatively estimating the accumulative damage induced by the earthquake and the tsunami in the whole bridge system with large caisson foundations.

Keywords: earthquake-induced damage; tsunami-induced wave impact; steel bridge; large caisson foundation; accumulative damage

1. Introduction

Recently, more and more steel bridges are employed at the port and offshore region (Altunisik *et al.* 2010, Olmati *et al.* 2013, Hu *et al.* 2015, Numan *et al.* 2016). However, these steel bridges are up against the damage obtained from strong earthquake and earthquake-induced secondary disasters. Some steel bridges don't collapse during strong earthquake, but collapse during the secondary disasters induced by the earthquake. For the offshore steel structures, the secondary disasters are most likely earthquake-induced tsunami. Fig. 1 is the global distribution map of tsunamis caused by different mechanisms, in which more than 80% tsunamis are caused by earthquake. It is concluded that the offshore structures are most likely subjected to both strong earthquake and earthquake-induced tsunami. During the 2011 Great East Japan earthquake occurring at the north-east pacific region, serious secondary disasters caused by collision of drifting containers or ships occurred in various structures when tsunami came (Ge *et al.* 2013, Kang *et al.* 2017). Numerical simulations of a long-span cable-stayed

steel bridge subjected to both strong earthquake and drifting object impact due to tsunami flow, in which it is assumed that the tsunami is caused by the earthquake, have been carried out using a novel evaluated method proposed in previous studies (Ge *et al.* 2013, Kang *et al.* 2017), where the combined earthquake-tsunami effect is taken into account to evaluate the accumulated earthquake-tsunami damage of a long-span cable-stayed steel bridge subjected to both the strong earthquake and the drifting object impact due to earthquake-induced tsunami flow (Kang *et al.* 2017). Tsunami propagation analyses are carried out by assuming that four earthquakes occur simultaneously. A series of seismic response analysis and impact analysis are carried out, and the damage to the main tower of bridge is evaluated by means of elastic-plastic finite element analysis. The previous study shows that piers of main tower of steel bridge can be severely damaged due to the combined earthquake-tsunami effect compared to only impact effect. All of strains, stresses, displacements and damages of the whole bridge induced by earthquake before the drifting object impact due to tsunami flow are considered to be initial conditions during the impact analysis. However, the tsunami-induced wave impact force on the steel bridge with large caisson foundations is not considered in the previous study. For some structures such as tide wall, the tsunami-induced wave impact force cannot

*Corresponding author, Professor,
E-mail: gehanbin@meijo-u.ac.jp

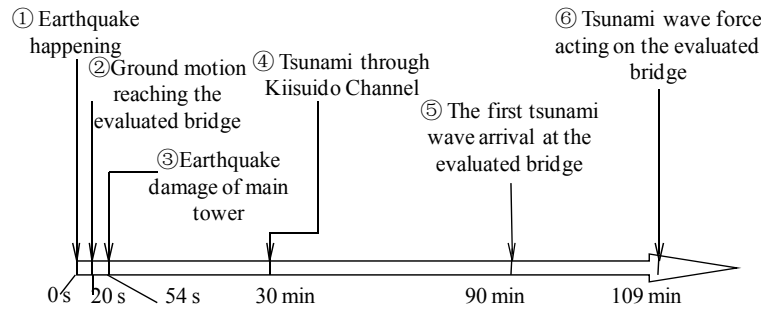


Fig. 4 Order of different actions applied on evaluated bridge in Osaka Gulf

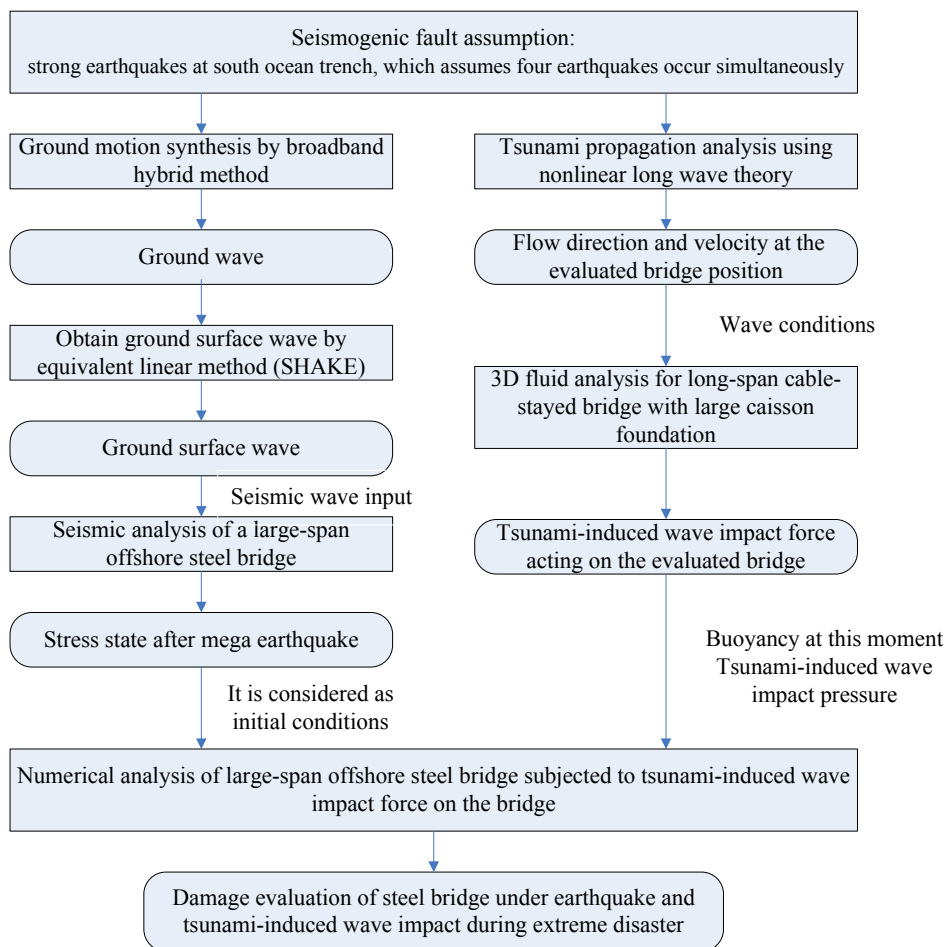


Fig. 5 Flowchart of damage evaluation for long-span offshore steel bridge subjected to actions including earthquake and following tsunami-induced wave impact force

2. Outline of study procedure

This study investigates the accumulative damage of a steel bridge located in Osaka Gulf subjected to earthquake and tsunami-induced wave impact. And the tsunami propagation analysis and earthquake response analysis are stated in chronological order as shown in Fig. 4.

- (1) Earthquake happening: 0 s
- (2) Ground motion reaching the evaluated bridge: 20 s
- (3) Earthquake-induced damage of main tower: 54 s
- (4) Tsunami through Kiisuido Channel: 30 min

- (5) The first tsunami wave arrival at the evaluated bridge: 90 min
- (6) Tsunami-induced impact wave force acting on the evaluated bridge: 109 min

In this study, the time of step (2) is estimated based on the distance (160 km) between the Tonankai earthquake fault position and the evaluated bridge position, and the S wave velocity (V_s) of 3.8 km/s. The time of step (3) is determined by the occurrence time of maximum accelerations in the X- and Y-directions during the earthquake response analysis of group motion source. The

Table 1 Assumed mega earthquake fault parameters and earthquake magnitude scale

Earthquake type	Fault position	Fault length L (km)	Fault width W (km)	Fault area S (km ²)	Moment magnitude M_w
Strong earthquakes at southern ocean trench	Tokai earthquake	115	82	9400	8.2
	Tonankai earthquake	174	91	15800	8.4
	Nankai earthquake	295	125	37000	8.8
Hyuganada earthquake	North	64	48	3082	7.7
	South	75	54	4079	7.8
Four earthquakes occurring simultaneously					9.0

times of steps (4)–(6) are from the tsunami propagation analysis.

In order to simulate such a series of complex phenomena, the procedure of this numerical investigation is described as follows:

- Tsunami propagation analysis is carried out based on the assumed earthquake source by using nonlinear long wave theory.
- The flow velocity and direction obtained from tsunami propagation analysis are regarded as the initial conditions, in which 3D fluid analysis is conducted by using OpenFOAM; and the wave pressure due to tsunami flow acting on the large caisson foundation is calculated.
- Depending on the above assumed seismic source model, the empirical Green's function is employed to simulate the short-period ground motions, and the 3D finite-difference method is used to determine the long-period ground motions from source faults (Kang *et al.* 2017). The seismic wave under such ground motions is inversed using equivalent linear method (SHAKE).
- Considering the interaction between the soil and fiber element model of the whole bridge with large caisson foundation, the accumulative damage of bridge is obtained by conducting nonlinear dynamic response analysis under such input ground motion.
- Based on the damaged state caused by earthquake, the impact analysis (elastic-plastic finite element analysis) is performed by inputting the tsunami-induced wave.

The procedure is illustrated in Fig. 5, where the earthquake source assumption in (a) and the details of 2D tsunami propagation analysis in (c) were stated in the references (Magoshi *et al.* 2013, Kang *et al.* 2017).

3. Tsunami propagation analysis

Tsunami propagation analyses are carried out by using tsunami wave source model proposed by the investigation

committee on models of strong earthquakes at southern ocean trench. This model assumes that the four earthquakes occur simultaneously ($M_w = 9.0$). Table 1 lists the information of the assumed strong earthquake. Table 2 lists the tsunami propagation analytical conditions, and the evaluated bridge is assumed to be located in the Osaka Gulf.

The tsunami propagation analysis is similar to that in previous research (Kang *et al.* 2017). The analytical area and mesh size can refer to the previous study. All of terrain data is provided by Japan Hydrographic Association and Geospatial Information Authority of Japan, and the data between meshes can be obtained by interpolation. The total analytical time is 360 minutes, and 0.1s is selected as the interval of analytical time. Manning's friction coefficient of sea bottom is 0.025. Besides, the mean half-monthly rising tide level of water close to the bridge during typhoon season T.P. +0.9 m (O.P. +2.20 m) is considered.

The contour map of water level change in Osaka Gulf and the horizontal vector diagram of flow velocity near the evaluated bridge at maximum flow is shown in Fig. 6. The tsunami reaches the Osaka Gulf from the Pacific Ocean

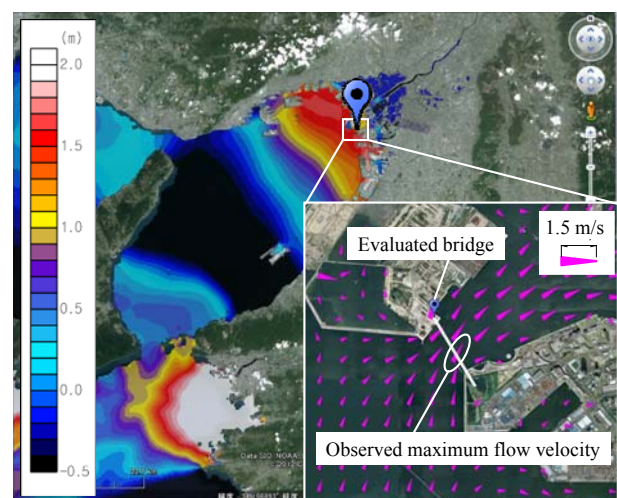


Fig. 6 Contour map of water level change in Osaka Gulf and horizontal vector diagram of flow velocity near evaluated bridge at maximum flow

though Kiisuido Channel 30 minutes after earthquake. Because the location of the evaluated bridge is inside the Osaka gulf and the tsunami-induced wave reflects from the complex geographical shapes, the wave height distribution is very difficult to be determined. Based on the tsunami propagation analytical results and the latest report published in Central Disaster Prevention Meeting, which was held on August 29th 2012, the maximum tsunami wave height of 1.3 m near the evaluated bridge calculated in this tsunami propagation analysis and the maximum tsunami wave height of 4 m that published in the above report are employed in different cases of the following 3D fluid analyses. The resultant flow velocity reaches to 1.14m/s 109 minutes later, and at that moment, the flow direction is 30.7°. Tsunami flow velocity, flow direction and tsunami wave height are regarded as the wave initial conditions during the following 3D fluid analysis.

4. 3D fluid analysis

The tsunami-induced wave impact force acting on the evaluated bridge with large caisson can be obtained through 3D fluid analysis based on the analytical results of 2D tsunami propagation analysis obtained from Section 3.

4.1 Analytical conditions

3D fluid analysis is conducted by employing the interFoam solver for 2 incompressible, isothermal immiscible fluids using a volume of fluid (VOF) phase-fraction based interface capturing approach in OpenFOAM. In this study, the large caisson foundation with cylindrical shape as shown in Fig. 3 is the evaluated object, besides, such cylindrical shape is benefit for using VOF method. The free surface is modeled using the VOF approach, and the turbulence closure is obtained using the standard TRANS model as well as with the dynamic Smagorinsky LES model. Around the caisson foundation, the pressure loss contains a complex evaluation, especially in the wake vortex flow.

In this study, the following two cases are considered:

- Case 1: assuming that the earthquake and tsunami come from the same fault motion, the tsunami height and flow velocity obtained from the above tsunami propagation analysis are regarded as the initial conditions of this 3D fluid analysis.
- Case 2: the earthquake and tsunami do not come from the same fault motion, the caisson foundation of steel bridge is assumed to be hit by a very large tsunami. The maximum tsunami height and flow velocity in the historical record are employed.

The two analytical cases are illustrated in Fig. 7. The effect of tsunami flow on the large caisson foundation is mainly investigated. The position of wave-making is T.P.+0.9 m of the caisson foundation.

The area of 3D fluid analysis is shown in Fig. 8. The foundation of the main tower P2 of steel bridge is regarded

as the center of area of 3D fluid analysis. The area is a 400 m × 800 m rectangular. Analytical boundary conditions are shown in Fig. 9. The side reflection boundary is indicated by the red solid line, the wave-making boundary is expressed by the blue solid line, and the radian boundary is indicated by the red dotted line. The effect of submarine topography is neglected. Analytical models including Cases 1 and 2 are illustrated in Fig. 10. The meshing of analytical models is listed in Table 2. In which, the mesh size of analytical models along both width and length directions is 2 m, and the mesh size of analytical models along height direction is 1 m. The number of total elements of analytical models for Cases 1 and 2 is 2,160,000 and 4,000,000,

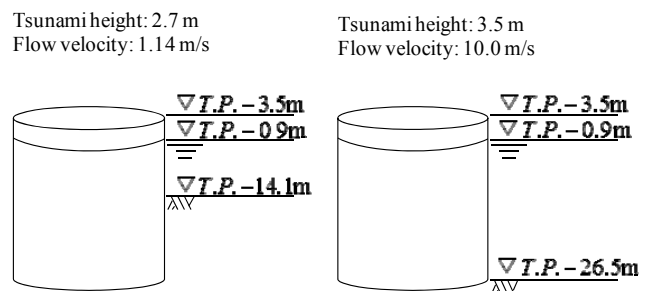


Fig. 7 Analytical cases

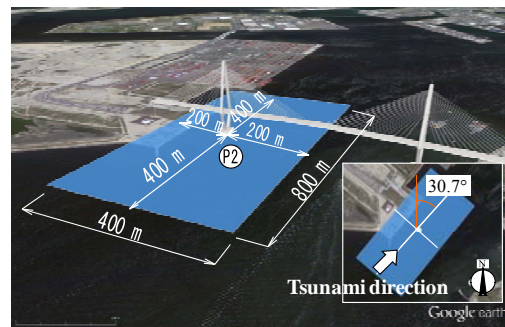


Fig. 8 Area of 3D fluid analysis

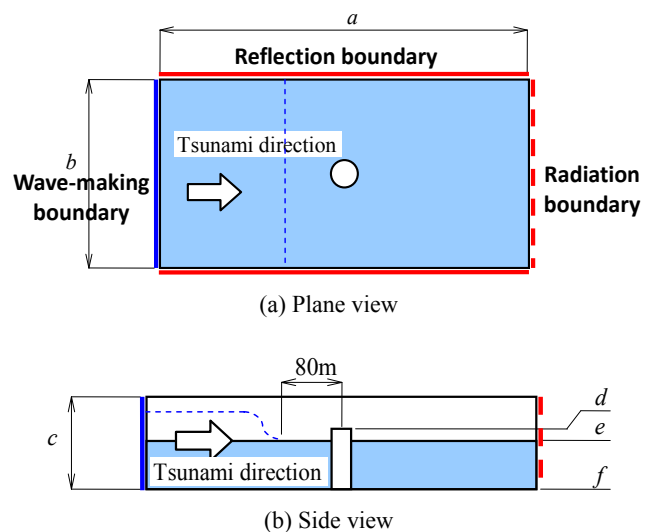


Fig. 9 Analytical boundary conditions

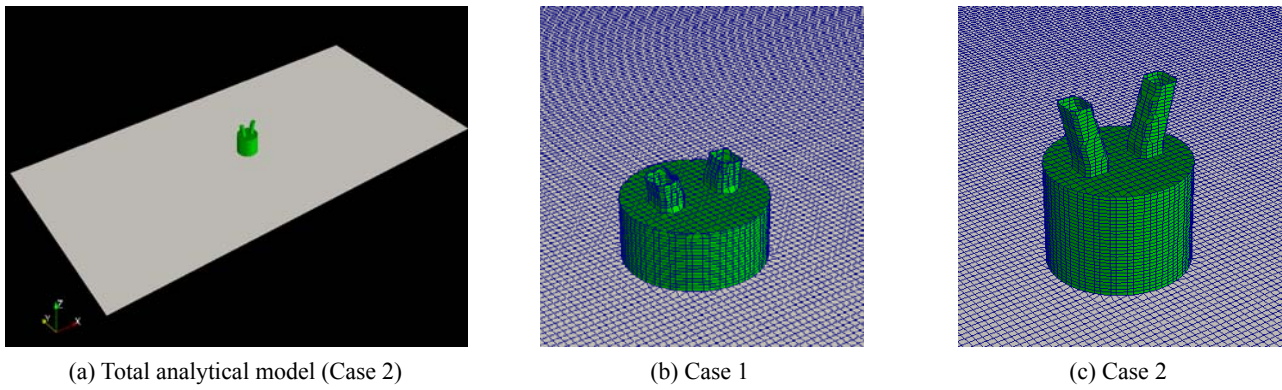


Fig. 10 Analytical model

Table 2 Mesh of analytical models

	Case 1	Case 2
a	2 m×400 = 800 m	2 m×400 = 800 m
b	2 m×200 = 400 m	2 m×200 = 400 m
c	1 m×27 = 27 m	1 m×50 = 50 m
d	T.P. +3.5 m	T.P. +3.5 m
e	T.P. +0.9 m	T.P. +0.9 m
f	T.P. -14.1 m (T.P. -22.6 m)	T.P. -26.5 m (T.P. -45.6 m)
Number of total elements	2,160,000	4,000,000

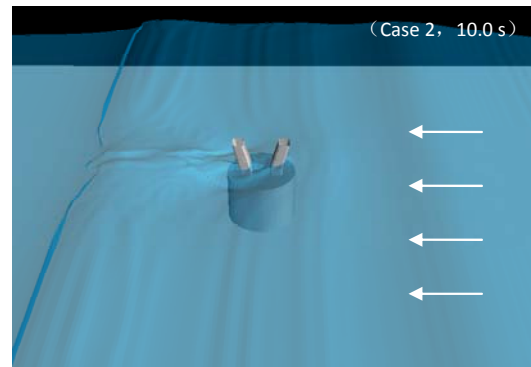


Fig. 12 Area of 3D fluid analysis (Case 2)

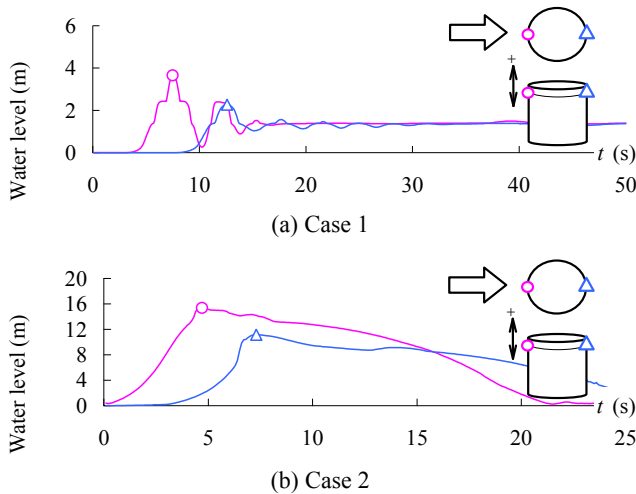


Fig. 11 Water level change in front and back of caisson foundation

respectively. The action due to tsunami flow is created by the tsunami flow 80 m away from the caisson foundation raising a height suddenly and then falling. The calculation interval time can be adjusted according to the calculation results, and initial interval time is 0.001 s.

The duration time of tsunami flow for Cases 1 and 2 is 50 s and 25 s, respectively. Because the flow velocity of Case 1 is relatively slow, the duration time of the tsunami flow for Case 1 is relatively long.

4.2 3D fluid analysis

The water level change in front and back of the caisson foundation is shown in Fig. 11. The tsunami direction is from the front of caisson foundation to the back of the caisson foundation. The initial tsunami level is zero. For the tsunami wave in Case 1, the water level of the front side of caisson foundation rises at 5.0 s, and that of the back side of caisson foundation begins to rise at about 8.0 s. At 8.0 s, the discontinuous rise of tsunami flow is captured because of local geometric discontinuity of caisson foundation. The tsunami wave acting on the caisson foundation at 10.0 s for Case 2 is illustrated in Fig. 12. The whole caisson foundation is completely submerged. The analytical results of 3D fluid analysis for Cases 1 and 2 are shown in Figs. 13 and 14.

5. Seismic response analysis

5.1 Full-period synthetic ground motion wave

A hybrid method for synthesizing ground motion wave in full-period is employed, similar to the previous studies (Magoshi *et al.* 2013, Kang *et al.* 2017). In which, the short-period ground motion wave (less than or equal to 1.0 s) is calculated by employing the statistical semi-empirical green function method, and the long-period ground motion wave (larger than 1.0 s) is calculated by the theoretical stiffness-matrix method (Dan and Sato 1998, Kawase and

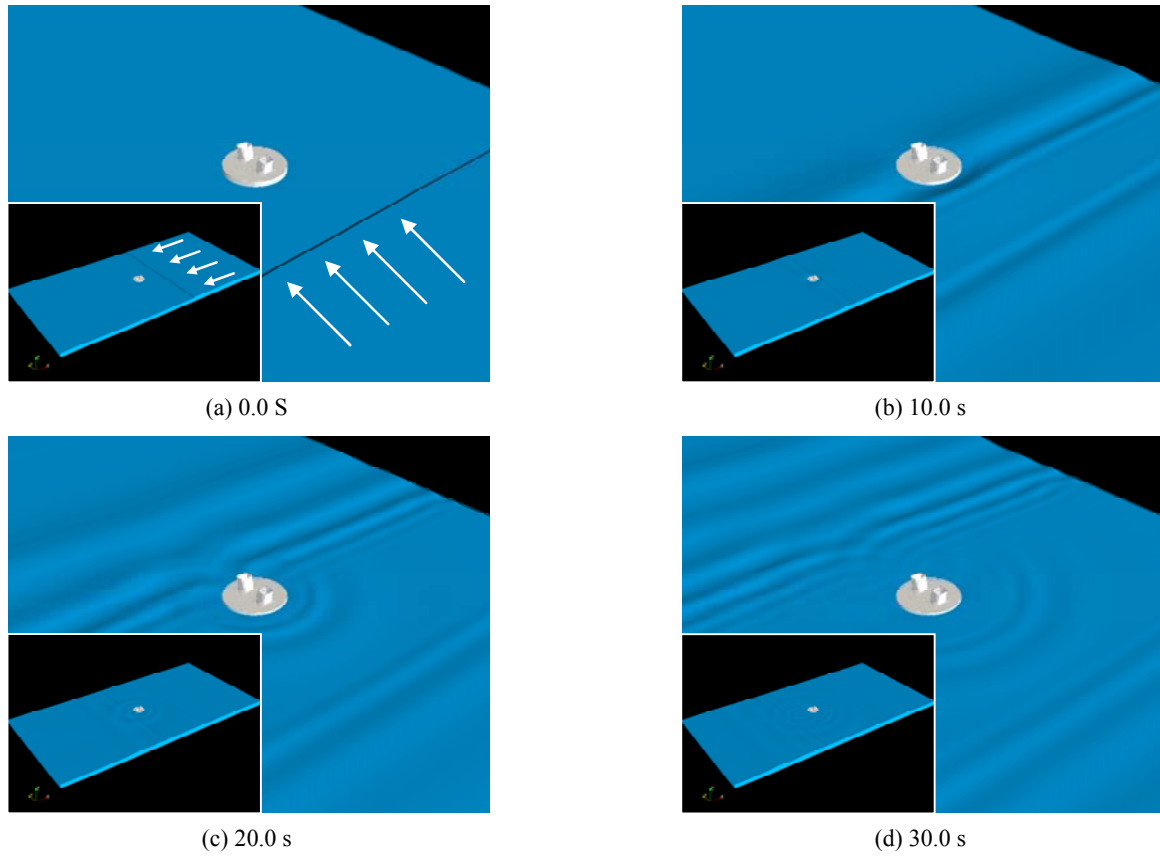


Fig. 13 Analytical results of 3D fluid analysis (Case 1)

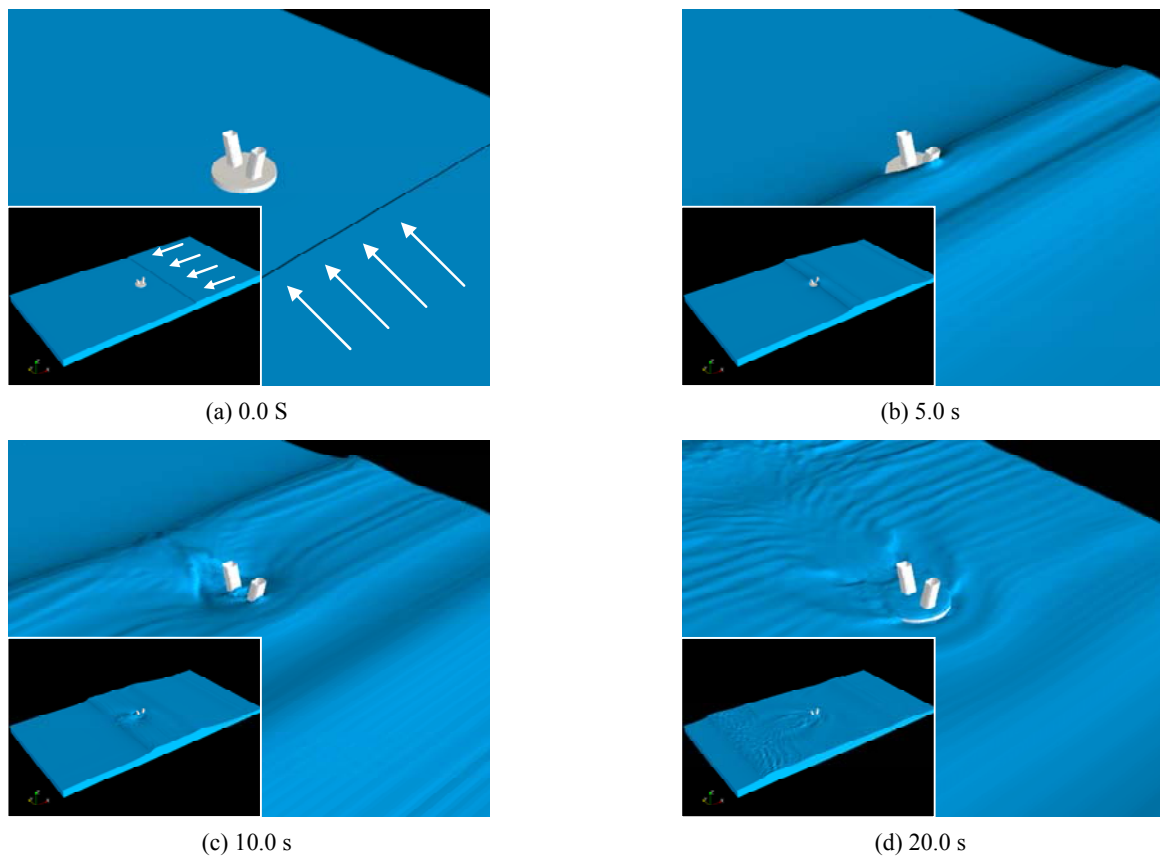


Fig. 14 Analytical results of 3D fluid analysis (Case 2)

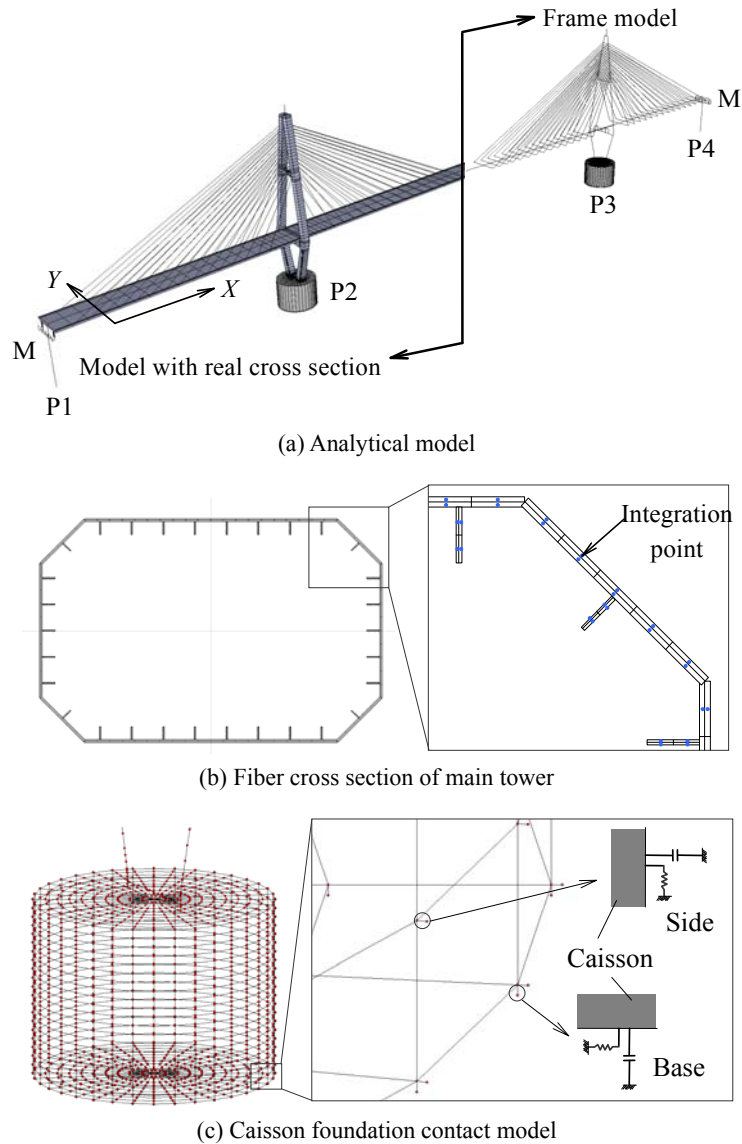


Fig. 15 Finite element analytical model of whole cable stayed bridge

Matsushima 1998, Yoshida *et al.* 2002, 2005). For the long-period ground motion wave during 1.0~1.2 s, a filtration is used to successfully connect such long-period ground motion wave with short-period ground motion wave. Finally, the surface ground motion response spectrum under such ground motion waves is synthesized employing the equivalent linear method.

5.2 Analytical model

Fig. 15(a) illustrates the finite element analytical model of the whole cable-stayed steel bridge (including the frame model in half and the model with real cross section in another half), which mainly includes elastic-plastic fiber beam nonlinear element and tension-only cable element. Fig. 15(b) illustrates the cross section of the main tower in fiber beam element. The material model employed in this study is bilinear hardening elastic-plastic model, and the plastic modulus is $E/100$ (E : elastic modulus). Moreover, the multi-node cable element is used to accurately predict

deflection and tension force during both the strong earthquake and the tsunami-induced wave impact. Analytical details can refer to the references (Nonaka and Ali 2001, Kang *et al.* 2017), as shown in Fig. 15(a), the longitudinal and transverse direction of the evaluated bridge are denoted as X- and Y-direction, respectively. The effect of large deformation is considered in seismic and tsunami-induced impact analysis of this study.

In this study, the caisson foundation contact model is shown in Fig. 15(c), in which the relationship between the caisson foundation and the soil of foundation bed is considered. The nonlinear model of ground reaction force as shown in Fig. 16 consists of normal and tangent direction. By employing this caisson foundation contact model, the contact properties between the caisson foundation and the soil of foundation bed (including uplift, peeling, sliding) can be characterized as three components along the contact surface, which can be simulated by the nonlinear springs.

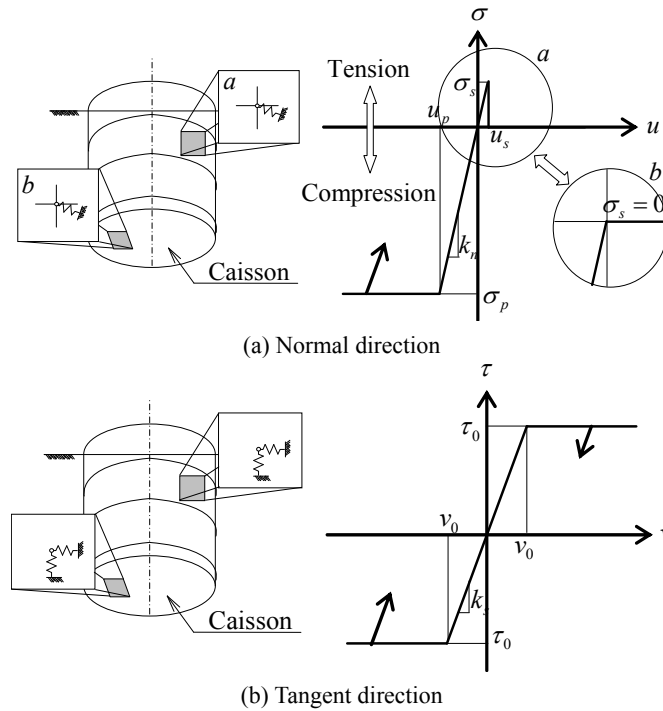


Fig. 16 Nonlinear model of ground reaction force

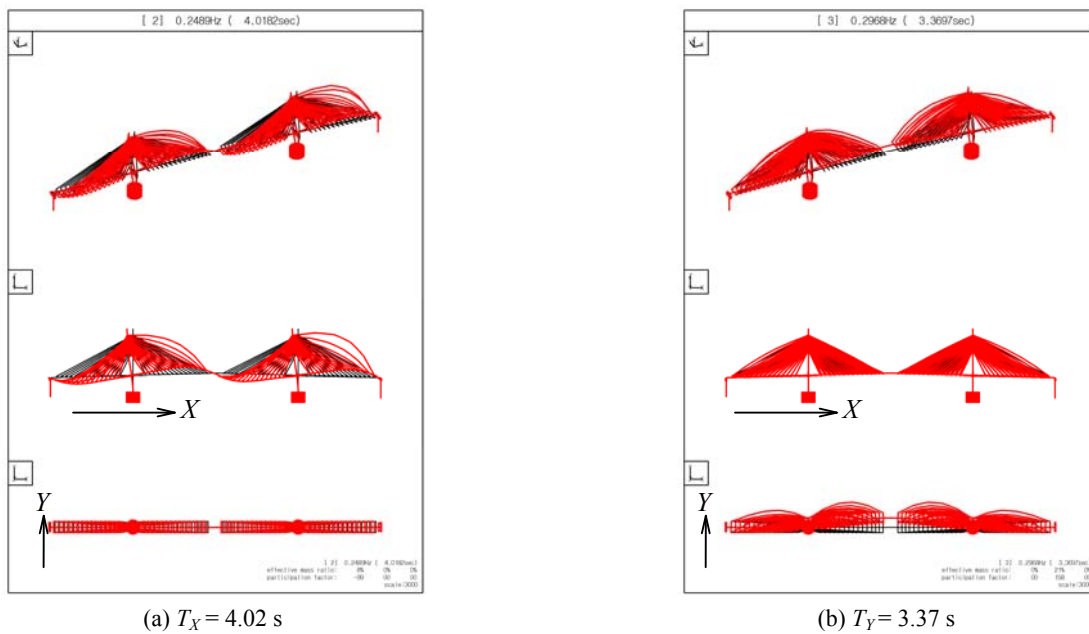


Fig. 17 Mode shapes of evaluated bridge

5.3 Eigenvalue analysis

Due to the results of eigenvalue analysis in this study, the mode shapes of the evaluated steel bridge in the longitudinal and transverse direction are shown in Fig. 17. The selected number of mode shapes should depend on the results of the seismic response analysis. The natural vibration periods of evaluated bridge in the longitudinal and transverse directions are $T_X = 4.02$ s and $T_Y = 3.37$ s, respectively. Meanwhile, the damping ratios corresponding to these mode shapes can be obtained.

5.4 Input seismic wave and analytical conditions

The longitudinal and transverse direction of the evaluated bridge is the input direction of the seismic wave. Fig. 18 plots the acceleration wave and the acceleration response spectrum of input seismic wave in X- and Y-direction (damping ratio is equal to 5%). In the acceleration waveform, the maximum accelerations in the X- and Y-direction is 391.5 gal and 335.3 gal (1 gal = 1.0 cm/s²), respectively, and the accelerations mainly distribute from 20 s to 150 s. The acceleration values corresponding to the

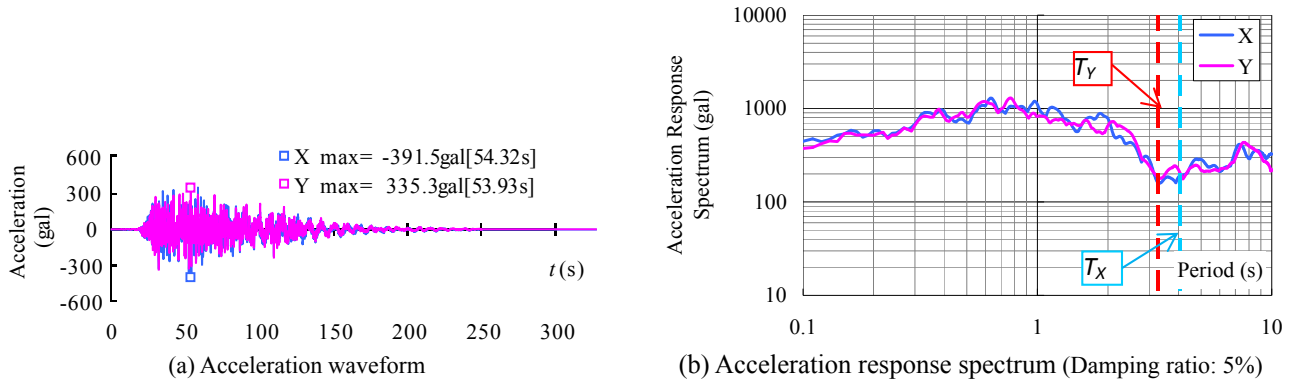


Fig. 18 Input seismic wave

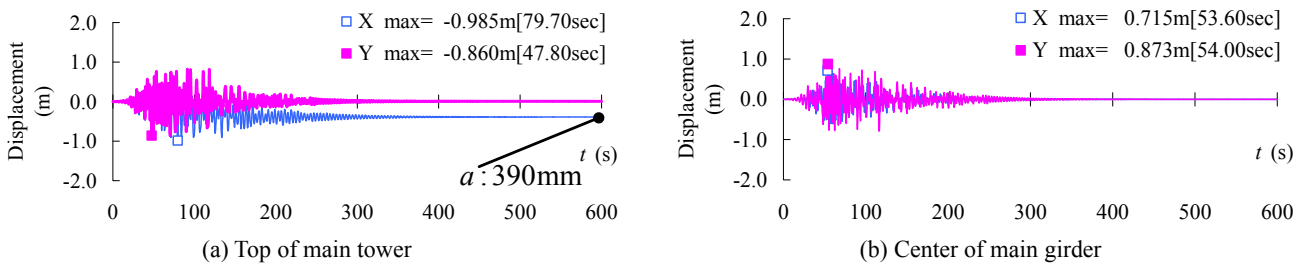


Fig. 19 Displacement-time histories

natural vibration periods T_X and T_Y are 187 gal and 180 gal, respectively. The input seismic waves consist of digital data with the same interval time of 0.01 s. Besides, the duration time of the input seismic waves is 300 s (5 minutes). In this study, the earthquake occurrence time is 0.0 s during input seismic wave.

The occurrence time of maximum velocity of tsunami-induced wave is 109 minutes later. The duration time of seismic wave is 300 s (5 minutes), the evaluated bridge with damping ratio of 0.05 converges to zero before tsunami-induced wave impact. The duration time of seismic

response analysis is taken as 600 s. The seismic response analysis is carried out by using finite element software SeanFEM ver.1.22.

5.5 Seismic response analysis

Fig. 19 demonstrates the displacement-time histories for the top of main tower P2 and the center of main girder in the offshore steel bridge. For the top of the main tower, the maximum displacements in X- and Y-direction are 0.985 m at 79.7 s and 0.860 m at 47.8 s, respectively. In addition, the

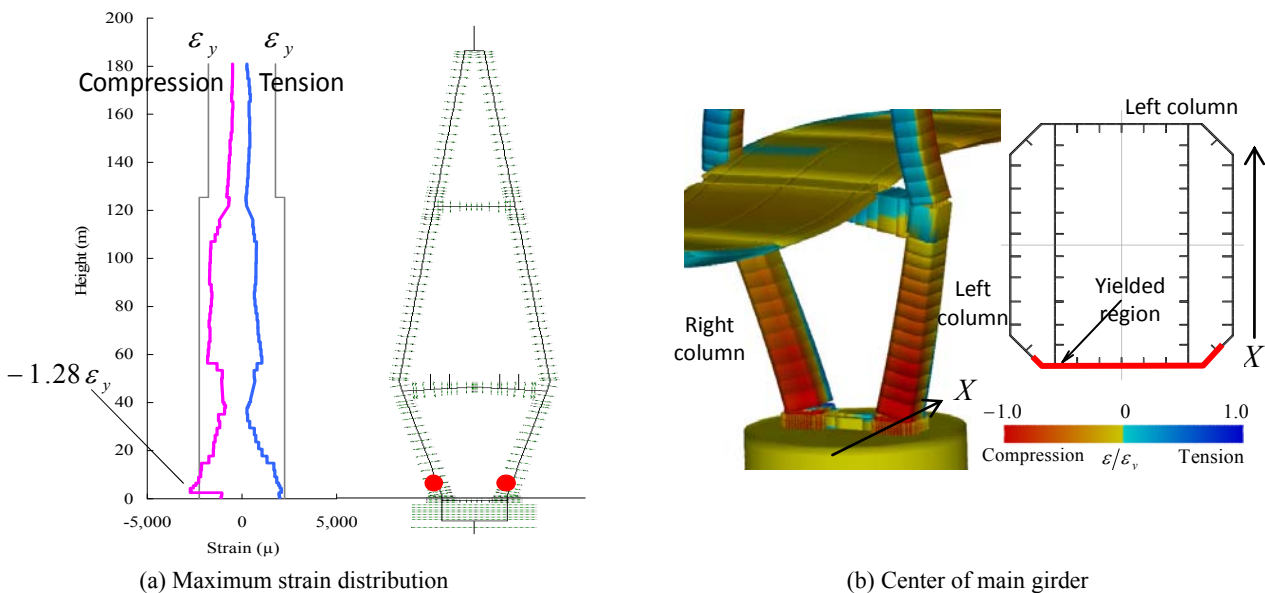


Fig. 20 Yielded region in cross section of right pier

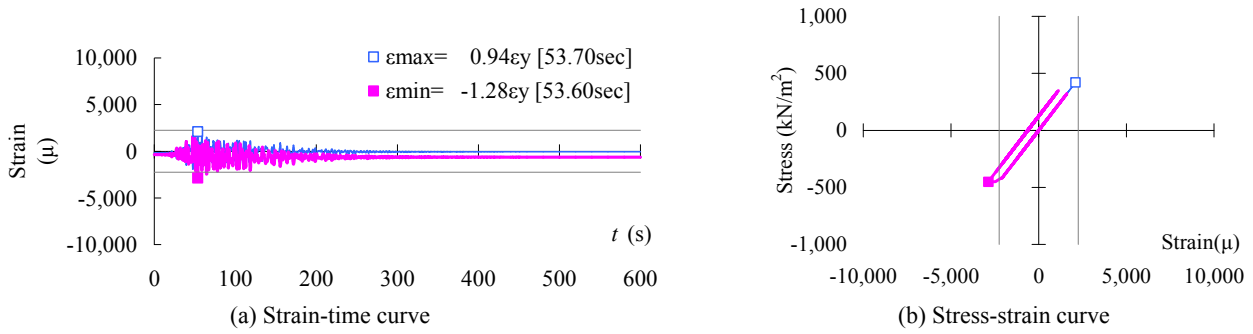


Fig. 21 Strain response of base of main tower P2

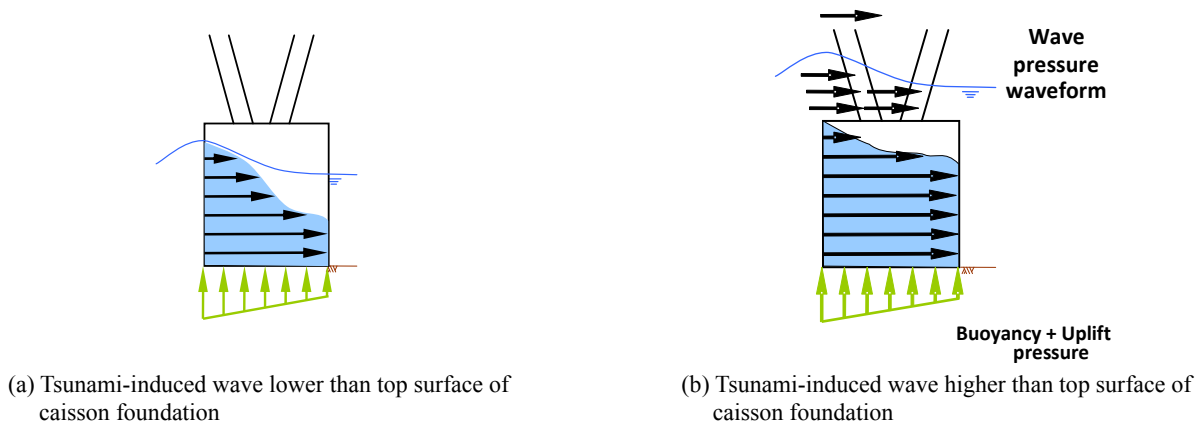


Fig. 22 Tsunami-induced waves

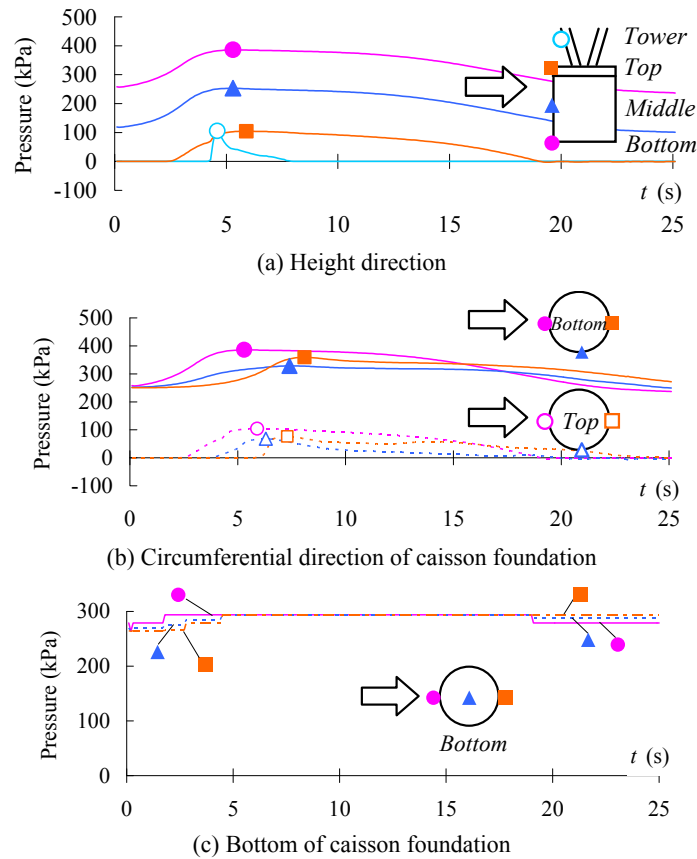


Fig. 23 Waveform of tsunami-induced wave pressure (Case 2)

main deformation state of the evaluated steel bridge in dynamic response is similar to the natural vibration mode shape as shown in Fig. 17(a). The maximum strain distribution of main tower and the yielded region in cross section of right pier due to the strong earthquake are shown in Fig. 20, in which compression strain is marked as the left purple line and tension strain is marked as the right blue line. The maximum strain appears at the bottom of main tower of offshore steel bridge. Meanwhile, the maximum strain ($= 1.28\varepsilon_y$, steel of SM570) occurs at the compression side of tower. Although the yielded region is less than the non-yielded region, there is the residual displacement of 390 mm at the top of main tower. Fig. 21 is the strain response of base of main tower P2. As shown in Fig. 21(a), the maximum strain is $0.94\varepsilon_y$, less than the yield strain, but the minimum strain is $-1.28\varepsilon_y$, more than the yield strain. It is concluded that the compression strain is more than tension strain. It is demonstrated that the yield state of bridge within the yielded region will be considered as the initial state during the following tsunami-induced wave impact analysis, and the tower pier within this yielded region might be in the damaged state firstly. Both the displacement and the strain of main tower P3 are symmetrical to those of main tower P2.

6. Tsunami-induced wave impact analysis

The residual stresses induced by the strong earthquake are used to the finite element model during the following tsunami-induced wave impact analysis as the initial stress

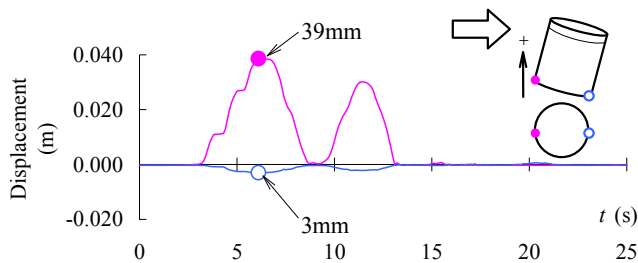


Fig. 24 Displacement-time history of caisson foundation subjected to tsunami-induced wave impact

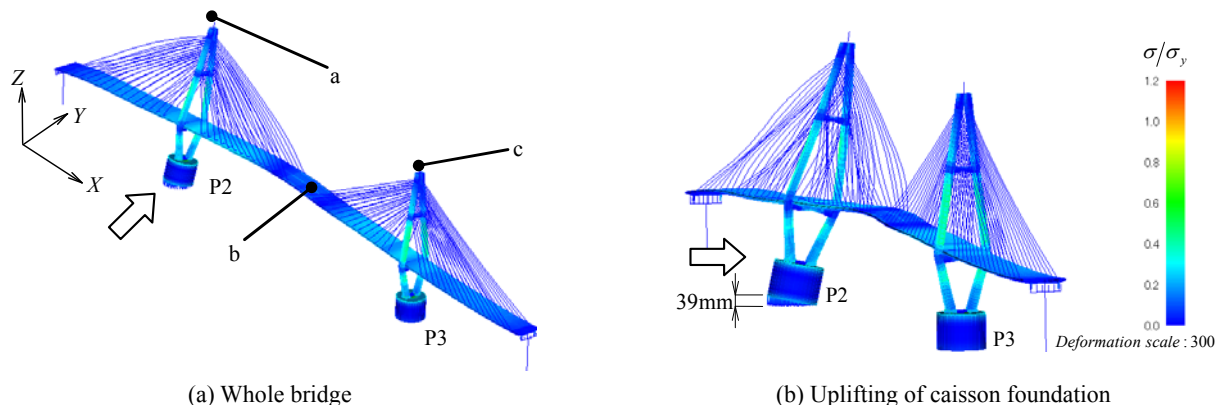


Fig. 25 Strain distribution and deformation of whole bridge subjected to tsunami-induced wave impact

state. The tsunami-induced wave obtained from Section 4 is employed. Fig. 22 illustrates the tsunami-induced waves in this study. The wave force of Case 2 is larger than that of Case 1, and the wave force of Case 2 is employed in this impact analysis.

6.1 Tsunami-induced wave force

The waveform of the tsunami-induced wave pressure (Case 2) is shown in Fig. 23. The tsunami-induced wave impact surface is the side surface of caisson foundation. The height of tsunami-induced wave is higher than the top surface of caisson foundation. In which, the P3 main tower is not subjected to wave impact at the same time. The tsunami-induced impact force applied on the whole bridge is asymmetry (Wang *et al.* 2016).

The foundation bed around the caisson foundation is assumed that there are pore waters between the foundation bed and the caisson foundation. Such pore waters lead to the pressure force of caisson foundation bottom and the buoyancy of caisson foundation. The water level change of front and back of caisson foundation leads to foundation rollover. All of these cause the upward pressure at the bottom of caisson foundation.

The arrow direction in Fig. 23 is the tsunami-induced wave direction. Pressure-time histories of different positions are given in this figure. The water pressure at 0 s in Fig. 23(a) is hydrostatic pressure, which increases with the increasing of water depth (represented as $\blacksquare \blacktriangle \bullet$ in this figure). Besides, the water pressure of the column of main tower around 4s is shown in Fig. 23(a) (represented as \circ in this figure). The tsunami-induced wave impact force applied to the structure is mainly due to the water level change at this moment. The water pressures of caisson foundation bottom and top are shown in Fig. 23(b). The tsunami-induced wave arrives the front of caisson foundation top (\circ in Fig. 23(b)) at about 3 s, and arrives the back of caisson foundation top (\square in Fig. 23(b)) at about 4 s. The water pressures of back, side and front of caisson foundation bottom (represented as $\blacksquare \blacktriangle \bullet$) are illustrated in Fig. 23(b). From the waveform of the tsunami-induced wave pressure at the bottom of caisson foundation as shown in Fig. 23(c), 90% of the caisson foundation is flooded. Accordingly, the water pressure of the bottom of caisson

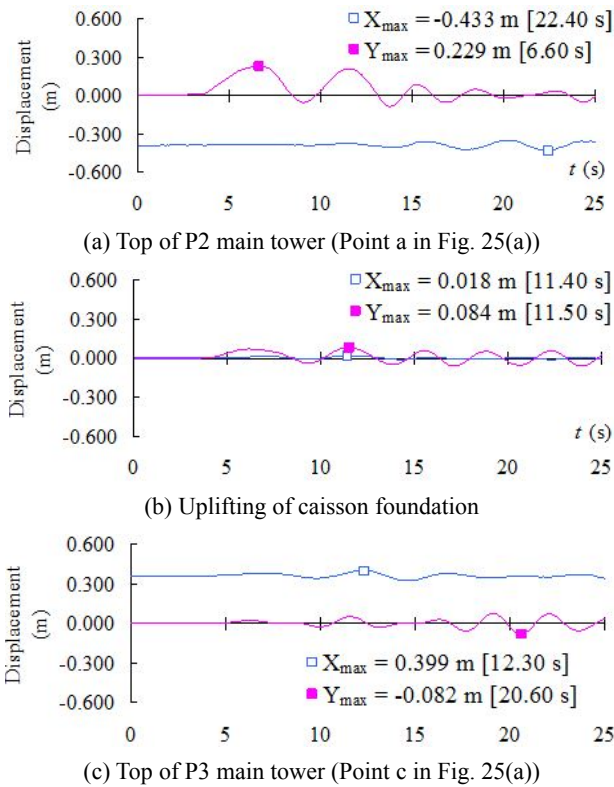


Fig. 26 Displacement-time histories of key points in evaluated steel bridge during tsunami-induced wave impact

foundation mainly is buoyancy. The sliding due to such buoyancy at the bottom of caisson foundation can be easily expressed, and its effect contributes to building the nonlinear model of ground reaction force. In detail, the sliding ultimate stress at the bottom of caisson foundation τ_0 can be calculated based on the Mohr-Coulomb's failure criterion, and the normal stress should be the buoyancy stress minus gravity stress. Here, the uplift pressure change with time can be neglected during calculating the sliding ultimate stress at the bottom of caisson foundation τ_0 . The interaction between the caisson foundation and the foundation bed, and the foundation sliding can be taken into account by employing such caisson foundation contact model and nonlinear model of ground reaction force.

6.2 analytical results

The displacement-time history of caisson foundation subjected to tsunami-induced wave impact is shown in Fig. 24. The maximum tilt of caisson foundation occurs at 6.2s, at this moment the strain distribution and the deformation of the whole bridge subjected to the tsunami-induced wave impact are shown in Fig. 25. The maximum vertical displacement of front point at caisson foundation bottom is 39 mm, and that of back point at caisson foundation bottom is 3 mm. Besides, the main deformation state of the evaluated bridge in the tsunami-induced wave impact analysis is similar to the natural vibration mode as shown in Fig. 17(a). The displacement-time histories of key points in evaluated steel bridge during tsunami-induced wave impact are plotted in Fig. 26. In general, the displacements obtained from the tsunami-induced wave impact analysis

are greatly less than those obtained from the former seismic analysis. The effect of tsunami-induced wave impact is that the plastic region of steel bridge is further enlarged. Besides, the residual displacement is the vertical displacement of front point at caisson foundation bottom of 39 mm due to the buoyancy, and no sliding at the bottom of caisson foundation is observed during analysis. It is concluded that the effect of tsunami-induced wave impact on the steel bridge with large caisson foundation is greatly less than that of the earthquake.

7. Conclusions

A numerical simulation for evaluating the accumulative damage of a cable-stayed steel bridge subjected to both strong earthquake and post-earthquake tsunami-induced wave impact is proposed in this study. The following conclusions can be obtained:

- (1) The tsunami-induced wave impact is determined by 3D fluid analysis. Different cases including the Case 1 assuming that the earthquake and the tsunami come from the same fault motion and the Case 2 assuming that the maximum tsunami height and flow velocity in the historical record are employed.
- (2) The numerical results of seismic response analysis in this study illustrates that the maximum strain ($= 1.28\varepsilon_y$, steel of SM570) occurs at the compression side of the tower, the yielded region is less than the non-yielded region, and some residual

displacements occur in the top of the main tower of the steel bridge.

- (3) Both the damage due to earthquake and the damage due to tsunami-induced wave impact are quantitatively considered in this study, and the final accumulative damage can be calculated based on the proposed method in this study. The damage due to the tsunami-induced wave impact is greatly less than the damage due to earthquake.
- (4) If the evaluated steel bridge did not collapse in the strong earthquake, the following tsunami-induced wave impact could not lead its collapse.

Future studies are underway by the authors to extend this numerical study to experimental investigation. Although there are many challenges of conducting experimental tests considering the accumulative effect, it may be necessary to characterize and simulate the accumulation damage by experimental method. The basic experimental investigations include the validity for the tsunami propagation analysis, the validation of the 3D fluid analysis, the benchmark study for the seismic structural analysis, and so on. The proposed method in this study is an attempt for evaluating the accumulative damage subjected to strong earthquake and tsunami-induced wave impact, however, the method may need revision based on future experimental results.

Acknowledgments

The study is supported in part by grants from the Advanced Research Center for Natural Disaster Risk Reduction, Meijo University, which supported by Ministry of Education, Culture, Sports, Science and Technology (MEXT), Japan. Besides, the authors also wish to thank the National Natural Science Foundation of China (Grant No. 51508205), the Science and Technology Planning Project of Guangdong Province of China (Grant No. 2014A020218002), and the Guangdong Province Special Support Program "Innovating Science and Technology for Young Top Talents" (2016TQ03Z528) for providing support for the authors to conduct this study.

References

- Altunisik, A.C., Bayraktar, A., Sevim, B., Kartal, M.E. and Adanur, S. (2010), "Finite element model updating of an arch type steel laboratory bridge model using semi-rigid connection", *Steel Compos. Struct., Int. J.*, **10**(6), 541-561. <http://dx.doi.org/10.12989/scs.2010.10.6.541>
- Asai, M., Miyagawa, Y., Idris, N., Muhari, A. and Imamura, F. (2016), "Coupled tsunami simulations based on a 2D shallow-water equation-based finite difference method and 3D incompressible smoothed particle hydrodynamics", *J. Earthq. Tsunami*, **10**(5), 1640019.
- Dan, K. and Sato, T. (1998), "Strong-motion prediction by semi-empirical method based on variable-slip rupture model of earthquake fault", *J. Struct. Constr. Eng. Architect. Inst. Japan, AIJ*, **509**, 49-60. [In Japanese]
- Ge, H.B., Kang, L. and Hayami, K. (2013), "Recent research developments in ductile fracture of steel bridge structures", *J. Earthq. Tsunami*, **7**(3), 1350021.
- Hanzawa, M., Matsumoto, A. and Tanaka, H. (2012), "Applicability of CADMAS-SURF to evaluate detached breakwater effects on solitary tsunami wave reduction", *Earth Planets Space*, **64**(10), 955-964.
- Hu, X., Xie, X., Tang, Z., Shen, Y., Wu, P. and Song, L. (2015), "Case study on stability performance of asymmetric steel arch bridge with inclined arch ribs", *Steel Compos. Struct., Int. J.* **18**(1), 273-288. <http://dx.doi.org/10.12989/scs.2015.18.1.273>
- Isshiki, M., Asai, M., Eguchi, S. and O-Tani, H. (2016), "3D tsunami run-up simulation and visualization using particle method with gis-based geography model", *J. Earthq. Tsunami*, **10**(5), 1640020.
- The OpenCAE Society of Japan (2010), OpenFOAM User Guide Ja-1.5. [Japanese Version]
- Kang, L., Magoshi, K., Ge, H.B. and Nonaka, T. (2017), "Accumulative response of large offshore steel bridge under severe earthquake and ship impact due to earthquake-induced tsunami flow", *Eng. Struct.*, **134**, 190-204.
- Kawase, H. and Matsushima, Y. (1998), "Strong motion simulation by a simulation by a semi-empirical method, a theoretical method and a hybrid method of the two - a case study on the 1995 Hyogo-ken Nambu earthquake", *Summaries of Technical Papers of Annual Meeting, AIJ*, **B-II**, 71-172. [In Japanese]
- Kihara, N., Niida, Y., Takabatake, D., Kaida, H., Shibayama, A. and Miyagawa, Y. (2015), "Large-scale experiments on tsunami-induced pressure on a vertical tide wall", *Coastal Eng.*, **99**, 46-63.
- Lau, T.L., Lukkunaprasit, P., Ruangrassamee, A. and Ohmachi, T. (2010), "Performance of bridges with solid and perforated parapets in resisting tsunami attacks", *J. Earthq. Tsunami*, **4**(2), 95-104.
- Liu, Q., Mo, Z., Wu, Y., Ma, J., Tsui, G.C.P. and Hui, D. (2016), "Crush response of CFRP square tube filled with aluminum honeycomb", *Compos. Part B-Eng.*, **98**, 406-414.
- Magoshi, K., Kang, L., Ge, H.B., Nonaka, T., Harada, T. and Murakami, K. (2013), "An evaluation method for large drifting object-bridge collision during tsunami", *J. Earthq. Tsunami*, **7**(2), 1350009.
- Mazinani, I., Ismail, Z.B. and Hashim, A.M. (2015), "An overview of tsunami wave force on coastal bridge and open challenges", *J. Earthq. Tsunami*, **9**(2), 1550006.
- Nonaka, T. and Ali, A. (2001), "Dynamic response of half-through steel arch bridge using fiber model", *J. Bridge Eng., ASCE*, **6**, 482-488.
- Nonaka, T., Motohashi, H., Yoshino, K., Harada, T., Kawasaki, K., Magoshi, K. and Sugatsuke, K. (2013), "3D tsunami simulations of wide region including a bridge using the K computer", *Proceeding of the 16th Symposium on Performance-based Seismic Design Method for Bridges*, Tokyo, Japan.
- Numan, H.A., Taysi, N. and Ozakca, M. (2016), "Experimental and finite element parametric investigations of the thermal behavior of CBGB", *Steel Compos. Struct., Int. J.*, **20**(4), 813-832. <http://dx.doi.org/10.12989/scs.2016.20.4.813>
- Olmati, P., Gkoumas, K., Brando, F. and Cao, L. (2013), "Consequence-based robustness assessment of a steel truss bridge", *Steel Compos. Struct., Int. J.*, **14**(4), 379-395. <http://dx.doi.org/10.12989/scs.2013.14.4.379>
- Perez, C.A. and Garcia, M.J. (2017), "Flow behaviour over a 2D body using the moving particle semi-implicit method with free surface stabilisation", *Int. J. Interactive Des. Manuf. (IJIDeM)*, **11**(3), 633-640.
- Sarjamee, S., Nistor, I. and Mohammadian, A. (2017a), "Large eddy simulation of extreme hydrodynamic forces on structures with mitigation walls using OpenFOAM", *Natural Hazards*,

- 85(3), 1689-1707.
- Sarjamee, S., Nistor, I. and Mohammadian, A. (2017b), "Numerical investigation of the influence of extreme hydrodynamic forces on the geometry of structures using OpenFOAM", *Natural Hazards*, **87**(1), 213-235.
- Triatmadja, R. and Nurhasanah, A. (2012), "Tsunami force on buildings with openings and protection", *J. Earthq. Tsunami*, **6**(4), 1250024.
- Usman, F. and Rahim, S.E. (2017), "Investigate the effectiveness of seawall construction using CADMAS Surf 2D", *MATEC Web of Conferences*, **97**, 01065.
- Wang, Y., Qian, X., Liew, J.Y.R. and Zhang, M.-H. (2016), "A numerical and theoretical investigation on composite pipe-in-pipe structure under impact", *Steel Compos. Struct., Int. J.*, **22**(5), 1085-1114.
<http://dx.doi.org/10.12989/scs.2016.22.5.1085>
- Wijatmiko, I. and Murakami, K. (2010), "Three dimensional numerical simulation of bore type tsunami propagation and run up on to a dike", *J. Hydrodynamics*, **22**(5), 259-264.
- Wu, Y., Liu, Q., Fu, J., Li, Q. and Hui, D. (2017), "Dynamic crash responses of bio-inspired aluminum honeycomb sandwich structures with CFRP panels", *Compos. Part B-Eng.*, **121**, 122-133.
- Yoshida, N., Kobayashi, S., Suetomi, I. and Miura, K. (2002), "Equivalent linear method considering frequency dependent characteristics of stiffness and damping", *Soil Dyn. Earthq. Eng.*, **22**(3), 205-222.
- Yoshida, N., Shinohara, H., Sawada, S. and Nakamura, S. (2005), "Role of engineering seismic base layer on defining design earthquake motion", *Struct. Eng. Earthq. Eng., JSCE*, **28**, 170-176. [In Japanese]